PHILOSOPHICAL TRANSACTIONS OF THE ROYAL SOCIETY A MATHEMATICAL, PHYSICAL & ENGINEERING SCIENCES

Computations of violent surface motions: comparisons with theory and experiment

J. C. Rogers and W. G. Szymczak

Phil. Trans. R. Soc. Lond. A 1997 **355**, 649-663
doi: 10.1098/rsta.1997.0031

Computations of violent surface motions: comparisons with theory and experiment

By J. C. W. Rogers[1] and W. G. Szymczak[2]†

[1]*Department of Applied Mathematics and Physics, Polytechnic University, Brooklyn, NY 11201, USA*

[2]*Naval Surface Warfare Center, Silver Spring, MA 20903, USA*

A numerical implementation of a generalized hydrodynamics has been used to compute a number of violent surface motions (characterized by the collision of different portions of the free surface). For some of these motions, singular aspects of the surface evolution may be analysed theoretically. Comparisons of the output of the calculations with theoretical predictions are made for these cases. In a second test of the predictions of the generalized hydrodynamics, the evolution of a plume generated by underwater explosions is compared with a computed plume history. An important diagnostic tool for studying violent surface motions has been analysis of the sum of the kinetic and internal energies of the flow. Accordingly, we include some results of an investigation into mechanisms for energy dissipation, as well as a description of some relations between energy loss and modes of cavity collapse.

1. Introduction

A framework to deal with hydrodynamic phenomena which are difficult to treat in classical formulations has been developed and numerically implemented. This framework is referred to as the 'generalized formulation of hydrodynamics'. Here we will not describe the generalized framework or the numerical implementation in detail. Such descriptions may be found in Rogers (1978*a*, *b*), Rogers *et al.* (1990) and Szymczak *et al.* (1991, 1993). More recently, a code has been written to treat three-dimensional flows in generalized coordinates. Computations using this code have been described at a recent symposium on cavitation Szymczak *et al.* (1995). A complete description of the three-dimensional code may be found in Szymczak *et al.* (1997).

In this section we offer a summary of the algorithmic prescription for solving flow problems which constitute the generalized formulation of hydrodynamics. We will primarily pay attention to the 'physical' aspects of the flows which are not accounted for in the classical formulation of hydrodynamics. We will say a few words regarding why we have chosen *this* generalized formulation; obviously, the process of generalization can be continued indefinitely. It will be apparent from the comments in § 4, on mechanisms of energy dissipation, that the generalized hydrodynamics we offer still has many basic unsolved problems (as is the case also with classical hydrodynamics).

† Present address: Physical Acoustics Branch, Code 7131, Naval Research Laboratory, Washington, DC, 20375, USA.

Phil. Trans. R. Soc. Lond. A (1997) **355**, 649–663
Printed in Great Britain

The second section of the paper presents the results of some computations using the generalized hydrodynamics and compares them with theoretical predictions. The third section compares observed and calculated properties of plumes formed by underwater explosions. A unifying purpose of this paper is to build confidence in the generalized hydrodynamics we have developed as a reasonable approach to the treatment of a number of phenomena which fall outside the purview of classical hydrodynamics.

What makes the generalized hydrodynamics 'general' is that it recasts the physical system of an inviscid incompressible fluid, with a free surface and contained by rigid boundaries, as a set of conservation laws for mass and momentum, subject only to an upper constraint on the mass density. The 'conservation laws' are, in the presence of gravity,

$$\rho_t + \nabla \cdot (\rho \boldsymbol{u}) = 0, \tag{1.1}$$

$$(\rho u)_t + \nabla \cdot (\rho \boldsymbol{u}\boldsymbol{u}) = -\rho g k, \tag{1.2}$$

and the constraint is

$$\rho \leqslant \rho_0. \tag{1.3}$$

The 'pressure' does not appear here explicitly, but, as will be described below, only implicitly in the process of satisfying the constraint (Rogers 1978*a*).

Although cast as partial differential equations, (1.1) and (1.2) admit weak solutions which are not differentiable (Rogers 1978*a*). For weak solutions, $\boldsymbol{u}$ need not be continuous, and ρ need not even be bounded. The constraint (1.3) does not require that space be delineated into regions, separated by a sharp boundary, where either $\rho = \rho_0$ or $\rho = 0$, as is assumed in the classical theory. There is also the possibility of having regions $0 < \rho < \rho_0$, called 'sprays'; in these regions, there is no pressure. As we shall see below, the pressure only enters overall as a Lagrange multiplier when the constraint (1.3) is sharp, i.e. $\rho = \rho_0$.

Since the velocity field can be discontinuous, we have the possibility of collisions. A feature of our formulation is that collisions are assumed to be inelastic, introducing the possibility of energy loss and irreversibility for inviscid flows. This assumption is not necessary, but reasons for its suitability, in a first generalization of classical hydrodynamics, are provided in § 4 of the paper.

Another limitation is provided by the assumption that the system can be described by a single velocity field $\boldsymbol{u}$ at each point, that is, that a kinetic model is not needed. Especially for the spray region, this assumption may be called into question. In defence of this assumption, we cite a recent paper (Leung & Rogers 1997) in which solutions of a model Boltzmann equation with a simple interaction term evolve into solutions of (1.1) and (1.2).

The generalized hydrodynamics is stated in the form of an algorithm which carries us from the flow $(\rho^n, \boldsymbol{u}^n)$ at time t^n (the superscripts label the time) to the flow $(\rho^{n+1}, \boldsymbol{u}^{n+1})$ at time $t^{n+1} = t^n + \tau$. In this algorithm, the constraint (1.3) is satisfied by restricting ourselves to initial data with $\rho(x, 0) \leqslant \rho_0$ and by requiring that

$$\frac{\mathrm{d}\rho}{\mathrm{d}t} = \rho_t + \boldsymbol{u} \cdot \nabla\rho \leqslant 0, \quad \text{when } \rho = \rho_0. \tag{1.4}$$

In view of (1.1), this is equivalent to requiring that

$$\nabla \cdot \boldsymbol{u} \geqslant 0, \quad \text{when } \rho = \rho_0. \tag{1.5}$$

The first step of the algorithm solves (1.1) and (1.2) approximately, without the

constraint (1.5), for the time τ, yielding a flow $(\tilde{\rho}, \tilde{\boldsymbol{u}})$. One way of doing this is to let the distribution function $f(\boldsymbol{x}, \boldsymbol{v}, t)$ be the solution of a 'collisionless Boltzmann equation',

$$f_t + \boldsymbol{v} \cdot \nabla f - g \frac{\partial f}{\partial v_z} = 0, \tag{1.6 a}$$

with initial data

$$f(\boldsymbol{x}, \boldsymbol{v}, 0) = \rho^n(\boldsymbol{x}) \delta(\boldsymbol{v} - \boldsymbol{u}^n(\boldsymbol{x})). \tag{1.6 b}$$

In terms of $f(\boldsymbol{x}, \boldsymbol{v}, t)$, the intermediate 'convective' mass density and velocity can be calculated according to

$$\rho(\boldsymbol{x}, t) = \int f(\boldsymbol{x}, \boldsymbol{v}, t - t^n) \, \mathrm{d}\boldsymbol{v}, \tag{1.6 c}$$

and

$$\rho(\boldsymbol{x}, t) \boldsymbol{u}(\boldsymbol{x}, t) = \int \boldsymbol{v} f(\boldsymbol{x}, \boldsymbol{v}, t - t^n) \, \mathrm{d}\boldsymbol{v}. \tag{1.6 d}$$

By integrating (1.6 *a*) over all values of $\boldsymbol{v}$, we find that ρ and $\boldsymbol{u}$ given by (1.6 *c*) and (1.6 *d*) always satisfy (1.1). Multiplying (1.6 *a*) by $\boldsymbol{v}$, and integrating over all values of $\boldsymbol{v}$, we find that ρ and $\boldsymbol{u}$ also satisfy (1.2) *when the characteristics* $\mathrm{d}\boldsymbol{x}/\mathrm{d}t = \boldsymbol{u}(\boldsymbol{x}, t)$ *do not intersect (collide)*. Whether or not such collisions take place, we calculate values of the mass and momentum densities at the end of the convective step from

$$\tilde{\rho} = \int f(\boldsymbol{x}, \boldsymbol{v}, \tau) \, \mathrm{d}\boldsymbol{v}, \tag{1.7 a}$$

and

$$\tilde{\rho} \tilde{\boldsymbol{u}} = \int \boldsymbol{v} f(\boldsymbol{x}, \boldsymbol{v}, \tau) \, \mathrm{d}\boldsymbol{v}. \tag{1.7 b}$$

In the second step of the algorithm, excesses of $\tilde{\rho}$ over ρ_0 are removed, and the velocity $\tilde{\boldsymbol{u}}$ is simultaneously corrected, by solving a 'Stefan–Boltzmann' equation:

$$f_\alpha(\boldsymbol{x}, \boldsymbol{v}, \alpha) = \nabla^2 \left(f(\boldsymbol{x}, \boldsymbol{v}, \alpha) \frac{(\theta(\boldsymbol{x}, \alpha) - \rho_0)_+}{\theta(\boldsymbol{x}, \alpha)} \right), \tag{1.8}$$

where

$$\theta(\boldsymbol{x}, \alpha) = \int f(\boldsymbol{x}, \boldsymbol{v}, \alpha) \, \mathrm{d}\boldsymbol{v} \tag{1.9}$$

is the intermediate mass density and

$$f(\boldsymbol{x}, \boldsymbol{v}, 0) = \tilde{\rho}(\boldsymbol{x}) \delta(\boldsymbol{v} - \tilde{\boldsymbol{u}}(\boldsymbol{x})). \tag{1.10}$$

Here α is the 'fast time' describing a rapid diffusion of density excesses, and (1.8) is run to steady state. Integrating (1.8) over $\boldsymbol{v}$ leads to the nonlinear diffusion equation

$$\theta_\alpha(\boldsymbol{x}, t) = \nabla^2 (\theta(\boldsymbol{x}, t) - \rho_0)_+, \tag{1.11}$$

which is the equation governing a one-phase Stefan problem (Rubenstein 1971). The steady state value of θ is $\rho^{n+1}(\boldsymbol{x}) \leqslant \rho_0$. Integrating (1.11) over α yields

$$\rho^{n+1} = \tilde{\rho} + \nabla^2 H, \tag{1.12}$$

where

$$H(\boldsymbol{x}) = \int_0^\infty (\theta(\boldsymbol{x}, t) - \rho_0)_+ \, \mathrm{d}\alpha \tag{1.13}$$

satisfies the variational inequality

$$\nabla^2 H = \begin{cases} \rho_0 - \tilde{\rho}, & \text{if } H > 0, \\ 0, & \text{if } H = 0. \end{cases} \tag{1.14}$$

During the diffusion process, the intermediate velocity $\boldsymbol{\xi}(\boldsymbol{x}, \alpha)$ is given by

$$\theta(\boldsymbol{x}, \alpha)\boldsymbol{\xi}(\boldsymbol{x}, \alpha) = \int \boldsymbol{v} f(\boldsymbol{x}, \boldsymbol{v}, \alpha)\, \mathrm{d}\boldsymbol{v}. \tag{1.15}$$

Multiplying (1.8) by $\boldsymbol{v}$ and integrating over α gives us

$$\frac{\partial}{\partial \alpha}(\theta(\boldsymbol{x}, \alpha)\boldsymbol{\xi}(\boldsymbol{x}, \alpha)) = \nabla^2(\boldsymbol{\xi}(\boldsymbol{x}, \alpha)(\theta(\boldsymbol{x}, t) - \rho_0)_+). \tag{1.16}$$

When $\theta(\boldsymbol{x}, \alpha)$ is known, (1.16) is a linear parabolic equation for $\boldsymbol{\xi}(\boldsymbol{x}, \alpha)$. Let $\bar{\boldsymbol{u}}(\boldsymbol{x})$ be the velocity at the end of the diffusion process, that is,

$$\bar{\boldsymbol{u}}(\boldsymbol{x}) = \boldsymbol{\xi}(\boldsymbol{x}, \infty). \tag{1.17}$$

Integrating (1.16) over α leads to

$$\rho^{n+1}\bar{\boldsymbol{u}} = \rho\tilde{\boldsymbol{u}} + \nabla^2 \int_0^\infty \boldsymbol{\xi}(\boldsymbol{x}, \alpha)(\theta(\boldsymbol{x}, \alpha) - \rho_0)_+ \, \mathrm{d}\alpha. \tag{1.18}$$

We approximate (1.18) by replacing $\boldsymbol{\xi}(\boldsymbol{x}, \alpha)$ on the right-hand side by its terminal value $\bar{\boldsymbol{u}}$, as given in (1.17). Thus, we solve the linear elliptic equation

$$\rho^{n+1}\bar{\boldsymbol{u}} = \rho\tilde{\boldsymbol{u}} + \nabla^2(H\bar{\boldsymbol{u}}) \tag{1.19}$$

for the redistributed velocity field .

For classical fluid flows without collisions, the second step of the algorithm gives only contributions which are of higher order in τ, and may be omitted. However, when fluid surfaces collide, it is important. This step, which distinguishes our method from the 'volume of fluid' approach of Hirt & Nichols (1981) or Kothe & Mjolsness (1992), is mass conserving. Both the momentum redistribution (1.18) and its approximation (1.19) have the property that the global energy cannot increase, and may decrease, depending on the flow dynamics. The importance of the redistribution steps (1.12) and (1.19) has also been examined numerically in Szymczak (1994).

The final step of the algorithm carries us from $(\rho^{n+1}, \bar{\boldsymbol{u}})$ to $(\rho^{n+1}, \boldsymbol{u}^{n+1})$. This involves a correction of the momentum density so that the constraint (1.5) is satisfied. This is done by 'projecting' in $L_2(\{\boldsymbol{x} : \rho^{n+1}(\boldsymbol{x}) \geqslant \rho_0\})$ the momentum onto the set of momenta satisfying (1.5). The projection involves the addition of the gradient of a Lagrange multiplier to the momentum. Since the correction pertains to changes which have taken place over a time interval τ, it can be expected that the Lagrange multiplier is proportional to τ, and hence we write it as $-P\tau$:

$$\rho^{n+1}\boldsymbol{u}^{n+1} = \rho^{n+1}\bar{\boldsymbol{u}} - \begin{cases} \nabla(P\tau), & \text{if } \rho^{n+1} = \rho_0, \\ 0, & \text{if } \rho^{n+1} < \rho_0. \end{cases} \tag{1.20}$$

For classical flows, ∇P becomes the rate of change of the momentum density with time, and P is the pressure. We continue to call P the 'pressure' for generalized flows. For classical flows the projection of the momentum density gives a Poisson equation for P. For generalized flows we obtain instead the variational inequality

$$\nabla^2(P\tau) = \begin{cases} \rho^{n+1}\nabla \cdot \bar{\boldsymbol{u}}, & \text{if } P > P_{\mathrm{C}} \\ 0, & \text{if } P = P_{\mathrm{C}}. \end{cases} \tag{1.21}$$

Here, P_C is the cavitation pressure of the liquid (often taken to be zero). There is a further connection between P and the function H given in (1.14). This is discussed in Rogers (1978*a*). Additional details describing this step appear in Rogers *et al.* (1990) and Szymczak *et al.* (1993).

In our numerical implementation of the algorithm, we solve (1.1) and (1.2) by using a second-order Godunov method with monotonized upwind slope limiting (Davis 1988). In the second step of the algorithm, a piecewise linear finite-element discretization is used for the Laplacian and a constrained conjugate gradient method with preconditioning is employed to find H satisfying (1.14). The momentum redistribution is performed by first transforming (1.15) into a symmetric self-adjoint degenerate elliptic problem. A standard discretization yields a matrix equation which is efficiently solved using a diagonally preconditioned conjugate gradient method. For the final step, the velocity $\bar{\boldsymbol{u}}$ is projected onto its discretely divergence-free subspace at points where the inequality (1.5) becomes an equality. This step is discretized using a standard finite element method in which the pressure belongs to the space of continuous bilinear (in two-dimensional) or trilinear (in three-dimensional) functions. An analysis of this approximate projection method (when there is no pressure constraint) appears in Almgren *et al.* (1996). In general, when the pressure constraint is imposed the pressure is determined through the solution of a variational inequality. The spatially discretized problem becomes a linear complementarity problem which is solved using a constrained direction preconditioned conjugate gradient method described in Szymczak *et al.* (1993). The importance of using a discretization of the variational inequality for the pressure as opposed to simply truncating the solution to the linear problem has been discussed in detail in Szymczak *et al.* (1995).

Details of the numerical discretizations for the BUB2D code (two-dimensional or axially symmetric problems on a tensor product grid) have been given in the references (Rogers *et al.* 1990; Szymczak *et al.* 1993). The code BUB3D includes a capability for Lagrangian grid motion, as well as the ability to solve three-dimensional problems in generalized coordinates (Szymczak *et al.* 1997). These same references also include the treatments of rigid boundaries, as well as interfaces across which the pressure is prescribed. Some of the flows computed in §§ 2–4 involve these more general boundary conditions.

The outline of the generalized hydrodynamics given above is for inviscid flows without surface tension. Extensions to viscous flows and to fluids with surface tension have been described in Rogers (1992) and, in the case of viscosity, have been put in numerical form.

2. Comparison of computational and analytical results

In this section we subject our treatment to some severe tests by comparing its predictions with theoretical predictions in two different cases in which the surface is subjected to violent motion.

For the first example, we consider the collision of two concentric cylinders of incompressible liquid surrounded by a region $\rho = 0$. Initially, the cylinders are moving in the vertical direction only along the axis of symmetry. The top cylinder has radius 1 and is moving downward with velocity $v = -4.0$. The bottom cylinder has radius 2 and is moving upward with velocity $v = 1.0$. Both cylinders have unit height. The initial distance between the cylinders is 0.2, so that the time of impact is $t = 0.04$, (see figure 1).

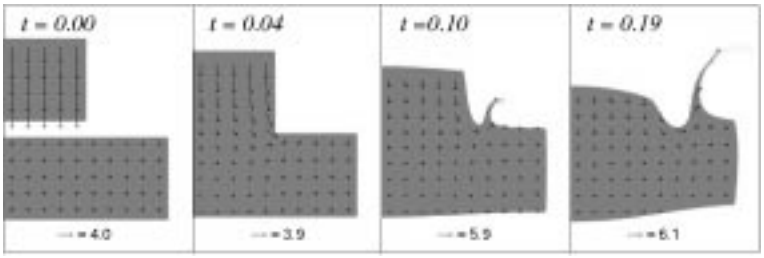

Figure 1. Greyscale density contours and velocity vectors of the collision of two concentric cylinders of an incompressible liquid. The medium grey colour represents densities $0.5 \leqslant \rho \leqslant \rho_0$. Lighter shades of grey correspond to $0 \leqslant \rho \leqslant 0.5\rho_0$, with white representing the region where $\rho = 0$.

Let us denote by z^* the value of z at which the cylinders make initial contact, and by R the union of the cylinders and their common surface at the moment of impact. At the instant of impact the momentum density of the fluid is changed impulsively by the amount ∇I, where I is the solution of the Dirichlet problem

$$\delta I = -5\rho_0\delta(z - z^*), \tag{2.1}$$

when $(r, z)\varepsilon R$, and

$$I = 0 \text{ on } \partial R. \tag{2.2}$$

It is easily seen that the singularity of ∇I at the circle $(1, z^*)$ is the same as the singularity of ∇I^* at $(1, z^*)$, where I^* is the solution of the Dirichlet problem

$$I^*_{rr} + I^*_{zz} = -5\rho_0\delta(z - z^*), \tag{2.3}$$

for $(r, z)\varepsilon R$, with the boundary conditions (2.2). A simple transformation that 'straightens out' the interior angle of $\frac{3}{2}\pi$ in R at $(1, z^*)$ shows that the momentum densities $-\nabla I$ and $-\nabla I$ are normal to ∂R on the boundary, and that their normal components can be written in the form

$$-\frac{\partial I}{\partial n} = A(r, z)((r - 1)^2 + (z - z^*)^2)^{-1/6}, \tag{2.4}$$

where $A(r, z)$, restricted to $(r, z)\varepsilon\partial R$, is continuous, and $A(1, z^*) > 0$. The velocity of the fluid emerging from points $(1, z > z^*)\varepsilon\partial R$ will be in the direction of increasing r, that from points $(r > 1, z^*)\varepsilon\partial R$ will be in the direction of increasing z. Elements of fluid from a neighbourhood of $(1, z^*)$ in ∂R will combine to form a stream moving upward and outward from $(1, z^*)$ at an angle of 45° in the (r, z) plane. The magnitude of the velocity at points in the combined stream will be proportional to the values of $-\partial I/\partial n$ at the points from which they originated at the instant of impact. Thus, according to (2.4), this magnitude will not be bounded uniformly for elements in the stream, but will behave like $d^{-1/3}$ where d is the distance from $(1, z^*)$ to the point on the surface from which each element originated.

In order to test this prediction, computer runs were made for five computational grids. The number of cells used for the grids was $N \times N$ with $N = 30$, 60, 120, 240 and 480. The cells were square and had size $h = 3/N$. Uniform time steps were taken with $\tau = 0.025$ h. Figure 1 shows greyscale density contours and velocity vectors (at every 16th cell) for the run with $N = 60$ at the initial time, time of impact, and at $t = 0.1$ and $t = 0.19$. A jet emerges from $(1, z^*)$ at the time of impact, as predicted.

A more quantitative comparison with the theory may be made by tabulating the maximum computed speed in the grid at the time of impact. Since the discrete

Table 1. *Maximum computed speeds for the collision problem*

N	$\max \lvert \boldsymbol{u}(t_0) \rvert$	rate
30	4.432	
60	6.226	0.490
120	8.964	0.526
240	11.555	0.366
480	15.059	0.382

velocities are located at cell centres, it is expected that the maximum computed speed at the time of impact will be proportional to $h^{-1/3}$, for sufficiently small h. The maximum speed V_h computed at the time of impact is shown in table 1 for each of the five grids, of size $h = 3/N$, employed. The 'rate' computed in the last column is simply $\log_2(V_h/V_2h)$. The computations give a value for this number which is slightly higher than the predicted value of $\frac{1}{3}$.

The energy lost upon impact of masses of fluid has been given for a class of such impacts in Rogers *et al.* (1990) and Szymczak *et al.* (1993). In the present case, this energy loss, per unit length, is

$$-\delta E = \tfrac{5}{2}\pi\rho_0 \int_0^1 I(r, z^*) r \, \mathrm{d}r. \tag{2.5}$$

(Note that our definition of I differs from that in the references by a factor ρ_0.) We have already computed the energy loss for the case of impact of cylinders of equal radii, and found the numerical value to agree well with the predicted value (Rogers *et al.* 1990; Szymczak *et al.* 1993; Szymczak 1994). We could compute the energy loss given by (2.5) also, but instead we have looked on the profile of energy as a function of time as a measure of the convergence of our computational results. For the case of impact of cylinders of equal radii, we found that the computed energy loss converged to the theoretical energy loss at a rate that was first order in h (and τ). Assuming that such a rate prevails in this case, we have plotted in figure 2 profiles of the energy as a function of time for four of the computations, and we have also given a profile extrapolated from the profiles for the computations with $N = 120$ and $N = 240$, based on the assumption of first-order convergence. For the time interval $0.04 \leqslant t \leqslant 0.3$, the extrapolated values had a minimum of 0.778 096, an average of 0.780 147 and a maximum of 0.781 057.

The second test of our numerical method concerns the flow generated by a wavemaker, which in this case is a wall moving impulsively into a fluid initially at rest and occupying a rectangular basin (in cross section). The reason for performing this test is that we have computed extensive profiles of breaking and splashing waves generated by a wavemaker (not shown in this paper), and we want to make some benchmark computations for such motions, in order to gain confidence in their accuracy. The number of theoretical predictions or experimental measurements with which we can compare our computational results is so far rather limited.

The calculations for the impulsively moving wall were performed using BUB3D, with a Lagrangian motion of the left wall. The results were made non-dimensional by selecting $\rho_0 = g = U = d = 1$, where g is the acceleration due to gravity, U is the uniform speed of the wall at the left and d is the initial water depth. Initially a

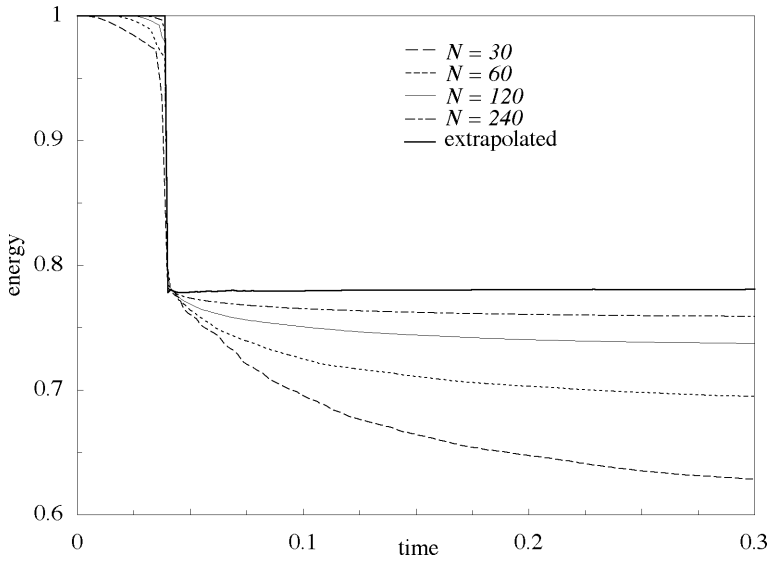

Figure 2. Computed energies for the collision problem. The extrapolated values were determined using the formula $E_{(\mathrm{extrap})}(t) = 2E_{(N=240)}(t) - E_{(N=120)}(t)$.

uniform grid of square cells was used in the region $0 \leqslant x \leqslant 1$ and $-1.0 \leqslant z \leqslant 0.5$. Due to the grid motion, the grid size in the x direction was reduced in time. Cell stretching was used in the x-direction for $1 \leqslant x \leqslant 10$. At the right boundary ($x = 10$), gridpoint velocities were extrapolated to zero and a hydrostatic pressure condition was imposed. Figure 3 displays computed contours of $\rho = 0.9\rho_0$ at time $t = 0.1$, using three different grids as well as predictions based on asymptotic approximations by Roberts (1987) and Joo *et al.* (1990). The configuration used in Roberts' study differs from ours, in that the initial water depth is infinite, but only the portion of the left wall with $-d \leqslant z$ is moved. King & Needham (1994) have discerned some faults in the early-time analysis of Joo *et al.* (1990) for the case of a uniformly accelerating wall. Roberts predicts a wave height at the left wall at time $t = 0.1$ of 0.384, while Joo *et al.* (1990) arrive at a value close to 0.4. On the finest grid we used (which still grossly under resolved the wave profile), the computed height was 0.358. The closer agreement at the wall using the coarser grids is merely fortuitous. Overall, the computed solutions appear to be approaching the asymptotic solutions, despite under resolving the wave profile.

3. Plume formation and evolution

A comparison with experiment has been made. Figure 4 shows photographs of the evolution of the plume formed by a shallow-depth explosion. Side-by-side with the photographs are computational results for the bubble evolution and plume formation and evolution, for the same times. The explosion bubble is modelled as an initially spherical region ($\rho = 0$), with volume V_0 and uniform pressure P_0. At later times the bubble pressure is determined using the adiabatic assumption $P_{\mathrm{B}}V_{\mathrm{B}}^{\gamma} = P_0V_0^{\gamma}$, where γ is the ratio of specific heats of the bubble gases. For the problem under consideration, the scaled depth, defined to be the initial charge depth divided by the maximum free field bubble radius, was 0.67. Figure 4 clearly shows that the plume's height and duration have been accurately reproduced. Note also the prediction of

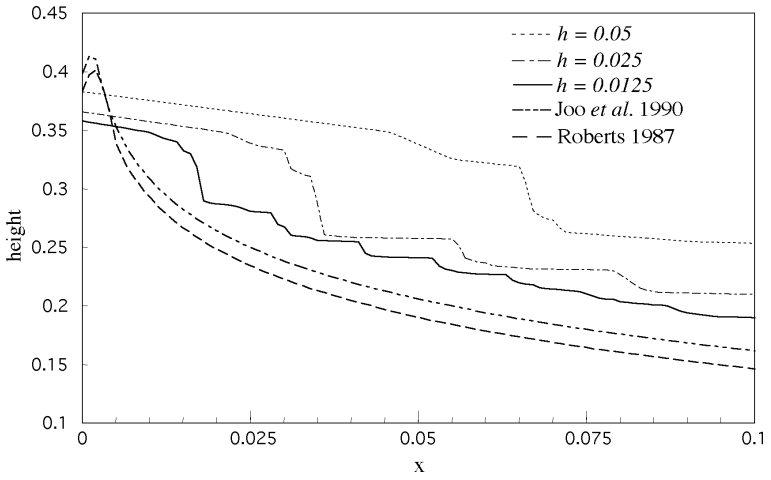

Figure 3. Computed free surface elevations adjacent to an impulsively started moving wall.

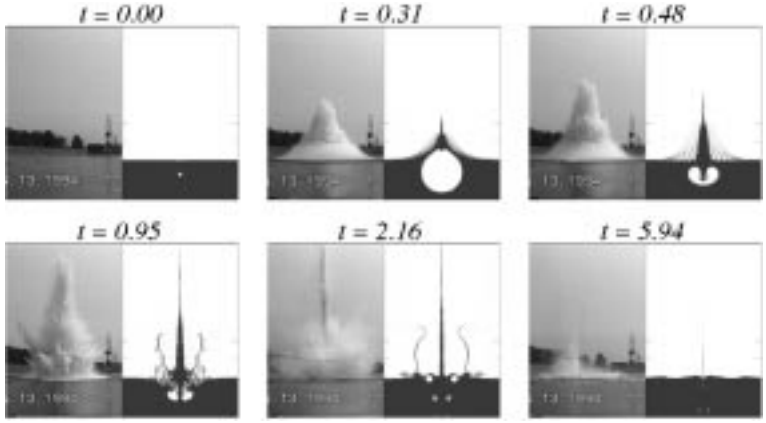

Figure 4. Photographs and computations of a shallow depth explosion.

the radial plumes ejected upon the bubble's second expansion as a toroidal region. The final time $t = 5.94$ is 11 times larger than the bubble period. The computation was performed using a 96×300 grid. About 4000 time steps were taken for the computation, which was executed in approximately 18 h on an HP 9000–735 work station. This problem has been studied in greater detail in Szymczak & Solomon (1996), where quantitative comparisons of the plume density are also made.

4. Causative factors for energy dissipation

As noted in the introductory section, kinetic energy loss is possible when portions of the fluid collide. Since energy loss does not occur for classical inviscid flows, the behaviour of the energy is an important indicator of the degree to which non-classical motions are taking place. Indeed, the behaviour of the total energy has also been used to test the convergence of the numerical procedure as the computational grid is refined. We have seen already an example of this in the study of the collision of cylinders of fluid of unequal radii in § 2.

The possibility of energy dissipation in collisions has been a source of contention in

some quarters, but some have accepted it as a reasonable representation of the physics of fluid collisions (Zhang *et al.* 1993). The question has been raised, quite naturally, whether energy loss would occur if one considered collisions of slightly compressible fluids, and then took the limit in which the sound speed became infinite.

To answer this question, we first recapitulate the one-dimensional incompressible flow given by solving (1.1)–(1.3) with $g = 0$ and with initial and boundary data

$$\rho(x,0) = \begin{cases} \rho_0, & \text{if } 0 < x < H, \\ 0, & \text{if } x > H, \end{cases} \tag{4.1}$$

$$\rho(x,0)u(x,0) = \begin{cases} -\rho_0, U & \text{if } 0 < x < H, \\ 0, & \text{if } x > H, \end{cases} \tag{4.2}$$

and

$$u(0,t) = 0. \tag{4.3}$$

These are the initial conditions for a flow which collides with the wall at $x = 0$ at time $t = 0^+$. For this flow, the generalized hydrodynamics says that the collision will be wholly inelastic, giving $\rho(x,t)u(x,t) = 0$ for $t > 0$. It is, of course, possible to imagine another solution of equations (1.1) and (1.2) (with $g = 0$) in which the flow for $t > 0$ consists of a slug of fluid of density ρ_0 and height H travelling to the right with speed U. This is the perfectly elastic case. Flows for which the evolution is intermediate between the perfectly elastic and perfectly inelastic extremes may also be constructed (Rogers 1977).

Now consider a compressible version of the incompressible collision. The initial and boundary conditions (4.1)–(4.3) remain, but (1.2) and (1.3) are replaced by

$$(\rho \boldsymbol{u})_t + \nabla \cdot (\rho \boldsymbol{u}\boldsymbol{u}) = -\nabla P, \tag{4.4}$$

and an equation of state linking P and ρ. Let us consider the case

$$P(\rho) = c^2(\rho - \rho_0)_+, \tag{4.5}$$

where $c > 0$ is constant, and let us obtain the solution to (1.1), (4.4), (4.5) with initial and boundary conditions (4.1)–(4.3) when $c > U$.

Defining ρ_1 and t_0 by

$$\rho_1 = \rho_0 \left(1 + \frac{U}{c}\right) \tag{4.6}$$

and

$$t_0 = \frac{H\rho_0}{c\rho_1}, \tag{4.7}$$

we have for the solution of the problem for $0 < t < t_0$:

$$\rho(x,t) = \begin{cases} \rho_1, & \text{for } 0 < x < ct, \\ \rho_0, & \text{for } ct < x < H - ut, \\ 0, & \text{for } x > H - Ut, \end{cases} \tag{4.8}$$

and

$$\rho(x,t)u(x,t) = \begin{cases} -\rho_0 U, & \text{if } ct < x < H - ut, \\ 0, & \text{elsewhere.} \end{cases} \tag{4.9}$$

Equations (4.8) and (4.9) describe a shock wave of strength U/c.

Corresponding to the pressure function (4.5), we find an internal energy per unit mass

$$e = \int -P(\rho)\,\mathrm{d}\left(\frac{1}{\rho}\right) = c^2\left(\ln\left(\frac{\rho}{\rho_0}\right) + \frac{\rho_0}{\rho} - 1\right). \tag{4.10}$$

At time $t = 0$, $e = 0$ in the flow, and the kinetic energy per unit mass is $\frac{1}{2}U^2$. At time t_0, there is no kinetic energy and the internal energy per unit mass is

$$c^2\left(\ln\left(\frac{\rho_1}{\rho_0}\right) + \frac{\rho_0}{\rho_1} - 1\right). \tag{4.11}$$

Expanding (4.11) in powers of U/c, we find that the total energy per unit mass at time t_0 is approximately

$$\frac{1}{U^2} - \frac{2U^3}{3c}.$$

That is, the sum of kinetic and internal energies per unit mass has its value reduced in the collision by a fraction $(4U)/(3c)$. This reduction is a familiar concomitant of shock waves (Landau & Lifshitz 1959), and the 'loss' of energy is generally identified with a production of entropy in the collision.

Continuing with the solution of equations (1.1), (4.4), and (4.5), we find, for $t_0 < t < 2t_0$,

$$\rho(x,t) = \begin{cases} \rho_1, & 0 < x < X_1(t), \\ \rho_1 \mathrm{e}^{-(x - X_1(t))/(c(t-t_0))}, & X_1(t) < x < X_2(t), \\ \rho_0, & X_2(t) < x < X_3(t), \\ 0, & x > X_3(t), \end{cases} \tag{4.12}$$

and

$$u(x,t) = \begin{cases} 0, & 0 < x < X_1(t), \\ \dfrac{x - X_1(t)}{t - t_0}, & X_1(t) < x < X_2(t), \\ c\ln\left(\dfrac{\rho_1}{\rho_0}\right), & X_2(t) < x < X_3(t), \end{cases} \tag{4.13}$$

where

$$X_1(t) = \frac{H\rho_0}{\rho_1} - c(t - t_0), \tag{4.14a}$$

$$X_2(t) = X_1(t) + c(t - t_0)\ln\left(\frac{\rho_1}{\rho_0}\right), \tag{4.14b}$$

$$X_3(t) = \frac{H\rho_0}{\rho_1} + c(t - t_0)\ln\left(\frac{\rho_1}{\rho_0}\right). \tag{4.14c}$$

As expected, the sum of kinetic and internal energies remains constant in this phase of the motion. If we continue the solution further in time, we eventually find a region bordering the wall at $x = 0$ in which $\rho(x,t) < \rho_0$ and the velocity $u(x,t) < c\ln(\rho_1/\rho_0)$. To the 'right' of this region we have $\rho(x,t) = \rho_0$ and $u(x,t) = c\ln(\rho_1/\rho_0)$.

In the whole process, only a fraction $(4U)/(3c)$ of the energy has been 'lost'. Thus, if we were to view our collision of an incompressible fluid as the limit, as $c \to \infty$, of

the compressible collision, we would be led to the case of perfectly elastic collision. That is, the fluid would 'bounce off' the wall.

However, suppose we were to view our connected incompressible flow as the limit of a compressible flow with N components separated by small interstices, as might happen when air is entrained with the liquid. Let the governing equations be (1.1), (4.4) and (4.5), and let the initial and boundary conditions be

$$\rho(x,t) = \begin{cases} \rho_0, & 0(i-1)(d+\eta) < x < (i-1)(d+\eta)+d, \quad 1 \leqslant i \leqslant N \\ 0, & \text{elsewhere,} \end{cases} \tag{4.15}$$

$$u(x,t) = -U, \quad \text{for } (i-1)(d+\eta) < x < (i-1)(d+\eta)+d, \quad 1 \leqslant i \leqslant N, \tag{4.16}$$

and

$$\rho(0,t)u(0,t) = 0, \tag{4.17}$$

where $d = H/N$. The width of each component is d and the interstices have width η. Suppose that U/c is small but finite, η/d is small, and $(dU)/(\eta c)$ is also small. Then in the time η/U that it takes for a component of fluid to travel the width of an interstice, a wave will have propagated across the width d and back. In the limit $c \to \infty$ the component for $i = 1$ will immediately reverse direction. At time $\tau = \eta/(2U)$ it will have traveled a distance $\frac{1}{2}\eta$ to the 'right' where it will be poised to collide with the component $i = 2$. Those two components will collide, almost elastically, and after an additional time τ the first component will be back at $x = 0$, ready to strike the wall, and the second component will be back at its original position, travelling to the right, and ready to collide with the third component. After time $2\tau i$, the first component will be ready to collide with the wall, the second and third components will be about to collide at $x = 2d + \eta$, the fourth and fifth at $x = 4d + 2\eta$, and the $2i$th and $(2i+1)$th components will be about to collide at $x = 2id + i\eta$. After time $(2i+1)\tau$, the first and second components will be ready to collide at $x = d + \frac{1}{2}\eta$, the third and fourth will be about to collide at $x = 3d + (\frac{3}{2})\eta$, and the $(2i+1)$th and $(2i+2)$th components will be about to collide at $(2i+1)(d+\frac{1}{2}\eta)$. The Nth component will collide at $(N-1)\tau$, and then will continue its motion away from the wall unimpeded. It will be followed by the $(N-1)$th component a time τ later, and so on. Eventually all the components will have reversed their initial velocity by time $2(N-1)\tau$. This is the picture if $U/c \to 0$ and N is finite.

Suppose, however, that U/c is small, but that $N(U/c)$ is large. A typical component will undergo $O(N)$ collisions with its neighbors. In each collision it will lose a fraction $O(U/c)$ of its energy. After N collisions the energy of the fluid will have been reduced by a factor $O(\exp(-\alpha NU/c))$, where α is a constant. Thus, for a sufficiently large N virtually all the energy will be lost.

Energy may be lost in a variety of modes. The initial and boundary conditions (4.1)–(4.3) can be considered to model the last stage of the collapse of a one-dimensional cavity. Similar models have been worked out for the collapse of a cylindrical and of a spherical cavity in Rogers (1977).

Consideration of the collapse of a cavity with walls which are only near planar leads us to expect that the one-dimensional cavity collapse described by (4.1)–(4.3) is really an approximation to a collapse in which numerous three-dimensional cavities are formed and collapse. Since the local energy concentrations are high in flows just before the collapse of a three-dimensional cavity (Rogers 1977), it is of some practical importance (for example, in predicting damage to structures in the water) to inquire as to how the energy is actually dissipated.

We remark that cavity collapse and the resulting collision of walls of fluid, as well as the collision of disconnected components of fluid, are all manifestations of Kelvin–Helmholtz instability, associated with loss of Lipschitz continuity in the velocity field. Kelvin–Helmholtz instability in its classical form, involving a vortex sheet, arises naturally out of collision phenomena. As an example, there may be a vortex sheet following the breakthrough of a re-entrant jet formed during the evolution of an underwater bubble (Zhang *et al.* 1993). Similar situations occur whenever 'Lagrangian points' run together (as when waves break, spill over, and impact on a water surface). The manner in which energy is dissipated by Kelvin–Helmholtz instabilities appears not to have been analysed in a satisfactory manner.

When cavities collapse completely, our generalized formulation of hydrodynamics predicts an energy loss, as described above, even though one might imagine other scenarios of elastic, or partly elastic, collapse and rebound. However, when the cavity does not collapse completely, our generalized formulation, like the classical treatments, will predict elastic rebound. This happens, for example, when there is a circulation about the cavity. If one studies the flow with circulation around a cylindrical cavity, it can be seen (Rogers 1977) that the cavity never collapses. Instead, for fluid occupying the region between two concentric cylinders, with the cross-sectional area of the region occupied by the fluid denoted by A, the circulation of the fluid around the inner cylinder denoted by C, the density of the fluid ρ_0 and the kinetic energy of the fluid per unit length denoted by E, we find for the minimum radius r_0 achieved by the inner cylinder in the course of the motion,

$$r_0 = \sqrt{\frac{A}{\pi}}(\mathrm{e}^{8\pi E/\rho_0 C^2} - 1)^{-1/2}. \tag{4.18}$$

Accordingly, when the circulation C is very small, the minimum radius r_0 becomes exponentially small and yet the cavity does not collapse. Hence this small amount of circulation has a big effect on the energy balance in the liquid.

At this point, the numerical implementation that we have devized for the generalized hydrodynamics, although not completely rigorous, can serve as a guide to what will happen. As an example, we consider what happens when a body of water in a vessel strikes a wall obliquely.

Our intuition about what happens when the free surface is tilted at an angle of 30°, with the wall against which it is to initially collide, is aided considerably by computation. Some computed solutions are displayed in greyscale contours in figure 5. The liquid region initially moves down with unit speed. The vessel has vertical walls on each side and a horizontal bottom. The time of initial impact is $t = 0.1$. After the tip of the liquid region touches the bottom wall, a horizontal jet moving from right to left appears in the frames labeled $t = 0.20$ and $t = 0.30$. This jet is turned upward after it strikes the left wall, as seen in the frame labeled $t = 0.41$. At $t = 0.52$ the cavity (modelled as a region of constant pressure) is near its minimum size and is surrounded by a strong recirculation of liquid. This recirculation causes the cavity to re-expand at later times, in accordance with the discussion preceding (4.18). The computational results depicted in figure 5 were computed using an 80×120 grid of uniform square cells of size $h = 1/80$. The computation was executed in approximately 70 min on an HP 9000-735 work station.

Figure 6 shows computed energy profiles for the calculation displayed in figure 5, and for computations performed on a coarser (40×60) grid and on a finer (160×240) grid. From the time $t = 0.1$ of first impact until the time that the horizontal jet

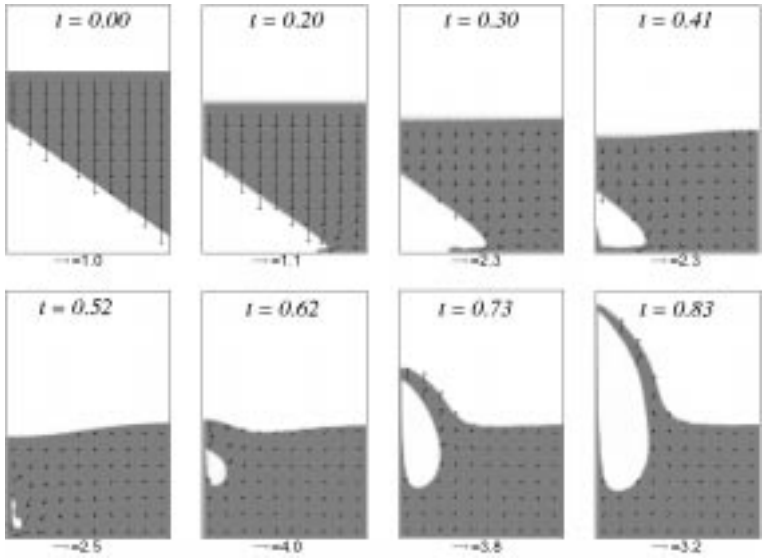

Figure 5. Computed density and velocity for the slanted impact problem. The computations were performed using a 80×120 grid.

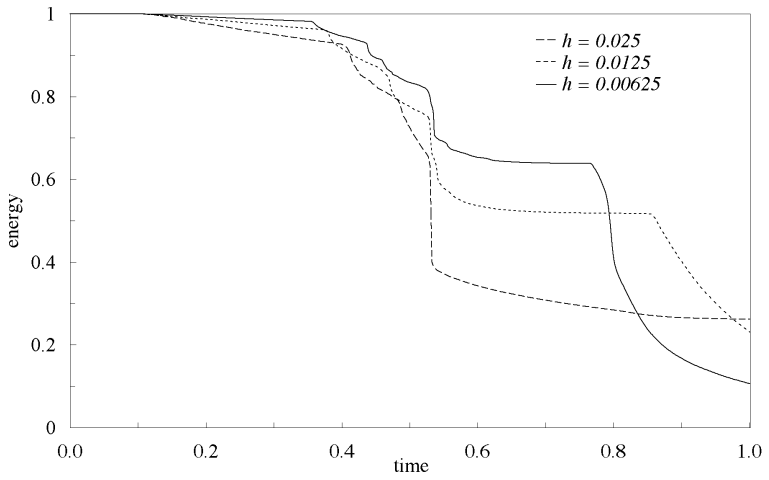

Figure 6. Computed energies for the slanted impact problem. Uniform grids of size $h = 1/N$ were used.

strikes the left wall, at $t \approx 0.4$, the energies decrease almost linearly with time, but the energy losses appear to converge to 0 as $h \to 0$. As the cavity shrinks, there appears to be substantial energy loss for $0.4 \leqslant t \leqslant 0.55$. After the re-expansion of the cavity, for $0.55 \leqslant t \leqslant 0.75$, the energy loss is negligible. The energy loss on the finer grids after $t = 0.75$ is due to the upper surface of the cavity impacting the top of the domain (also modelled as a solid wall).

The work of W.G.S. has been supported under the Independent Research program of the Naval Surface Warfare Center and by the Office of Naval Research, Code 311. The experimental tests shown in figure 4 were supported by the Office of Naval Research, Code 351. Both of us have a continuing indebtedness to our collaborators, A. E. Berger and J. M. Solomon, whose active

role in the development of the numerical methods used here will be evident from a perusal of the references.

References

Almgren, A. S., Bell, J. B. & Szymczak, W. G. 1996 A numerical method for the incompressible Navier–Stokes equations based on an approximate projection. *SIAM Jl Sci. Comput.* **17**, 358–369.

Davis, S. F. 1988 Simplified second order Godunov-type methods. *SIAM Jl Sci. Comput.* **9**, 445–473.

Hirt, C. W. & Nichols, B. D. 1981 Volume of fluid (VOF) method for the dynamics of free boundaries. *J. Comput. Phys.* **39**, 201–225.

Joo, S. W., Schultz, W. W. & Messiter, A. F. 1990 An analysis of the initial-value wavemaker problem. *J. Fluid Mech.* **214**, 161–183.

Kothe, D. E. & Mjolsness, R. C. 1992 RIPPLE: a new model for incompressible flows with free surfaces. *AIAA Jl* **30**, 2694–2700.

King, A. C. & Needham, D. J. 1994 The initial development of a jet caused by fluid, body and free-surface interaction. 1. A uniformly accelerating plate. *J. Fluid Mech.* **268**, 89–101.

Leung, S. & Rogers, J. C. W. 1997 A model Boltzmann approach for the collision of dilute gases. *Appl. Math. Letters.* (To appear.)

Roberts, A. J. 1987 Transient free-surface flows generated by a moving vertical plate. *Q. Jl Mech. Appl. Math.* **40**, 129–158.

Rogers, J. C. W. 1977 Some exact hydrodynamic flows with free surfaces. Johns Hopkins Applied Physics Lab. TG 1307.

Rogers, J. C. W. 1978*a* Incompressible flows as a system of conservation laws with a constraint. Seminaires IRIA Analyse et Contrôle de Systèmes. pp. 141–162.

Rogers, J. C. W. 1978*b* Stability, energy conservation, and turbulence for water waves. Seminaires IRIA Analyse et Contrôle de Systèmes. pp. 163–180.

Rogers, J. C. W. 1992 Aspects of nonclassical hydrodynamics. Talk given at *Conf. on Nonlinear Mathematical Problems in Industry, November 1992, Iwaki, Japan.*

Rogers, J. C. W., Szymczak, W. G., Berger, A. E. & Solomon, J. M. 1990 Numerical solution of hydrodynamic free boundary problems. *Free boundary problems, proceedings, conference on free boundary problems-numerical methods and optimal control* (ed. K.-H. Hoffmann & J. Sprekels), pp. 241–266. Basel: Birkhäuser.

Rubenstein, L. I. 1971 *The Stefan problem.* Providence, RI: AMS.

Szymczak, W. G. 1994 Energy losses in non-classical free surface flows. *Bubble dynamics and interface phenomena* (ed. J. R. Blake, J. M. Boulton-Stone & N. H. Thomas), pp. 413–420. Dordrecht: Kluwer.

Szymczak, W. G. & Solomon, J. M. 1996 Computations and experiments of shallow depth explosion plumes. Naval Surface Warfare Center, NSWCDD/TR–94/156.

Szymczak, W. G., Solomon, J. M., Berger, A. E. & Rogers, J. C. W. 1991 A numerical method based on a generalized formulation of hydrodynamic free surface problems. *AIAA 10th Computational Fluid Dynamics Conf., June 1991, Honolulu, Hawaii.*

Szymczak, W. G., Rogers, J. C. W., Solomon, J. M. & Berger, A. E. 1993 A numerical algorithm for hydrodynamic free boundary problems. *J. Comput. Phys.* **106**, 319–336.

Szymczak, W. G., Solomon, J. M., Berger, A. E. & Rogers, J. C. W. 1995 Numerical simulations of cavitation inception. *Proc. of CAV '95, The Int. Symp. on Cavitation, May, 1995, Deauville, France.* pp. 399–406.

Szymczak, W. G., Solomon, J. M. & Berger, A. E. 1997 BUB3D (description of mathematical model, algorithms, and user's guide). Naval Surface Warfare Center, NSWCDD/TR–95/42.

Zhang, S., Duncan, J. H. & Chahine, G. L. 1993 The final stage of the collapse of a cavitation bubble near a rigid wall. *J. Fluid Mech.* **257**, 147–181.